Visualising atmospheric mountain waves using sailplane flight data

G.D. Stirling[1], R.P. Millane[1], E. Enevoldson[2] and J.E. Murray[2]

[1]Dept. Electrical & Computer Engineering, University of Canterbury,
Private Bag 4800, Christchurch, New Zealand
[2]NASA Dryden Flight Research Center
PO Box 273, Edwards, CA 93523, USA
Email: rick@elec.canterbury.ac.nz

Abstract

Mountainous terrain can, under certain conditions, induce stationary atmospheric waves in the lee of the mountains, with large vertical air velocities. These waves are used as a source of strong lift by sailplane pilots. Methods are developed for inverting data of airspeed and GPS-derived position taken from sailplane data logs, to obtain estimates of the airmass vertical velocity in mountain waves. The method accounts for the static and dynamic aerodynamics of the sailplane and the effects of altitude. The airmass vertical velocity estimates are combined with estimates of the horizontal wind velocity to estimate the mountain wave structure and its relationship to the upwind topography. The methods are applied to data from a Perlan Project flight in the lee waves of the Sierra Nevada Mountain range in California.

Keywords: mountain waves, lee waves, sailplane, glider

1 Introduction

Under certain conditions, airflow passing over mountains can form standing atmospheric waves, which can have large vertical air velocities [1-4]. These disturbances extend into the troposphere and, under certain meteorological conditions, may extend into the stratosphere. These standing waves have a typical wavelength of 2-20km and decay approximately exponentially with distance downwind. By flying in the leading edge of these massive waves of air, sailplane pilots can soar to altitudes in excess of 40,000 feet. Wave soaring is now commonplace, and is the means by which many spectacular flights, both in altitude and distance, have been made.

Little quantitative data collection and analysis has been conducted on mountain wave systems. However, modern instrumentation can be used to obtain useful data from sailplane flights in mountain waves. This method of data collection has some advantages over weather balloons and radar, as a skilled pilot has the freedom to systematically explore the wave system. The advantage of using a sailplane over a powered aircraft is due to the simple aerodynamic forces acting on the sailplane compared to the more complex, and not as well characterised, forces acting on a powered aircraft.

We have previously described estimation of the horizontal wind velocity from sailplane flight data as well as rough estimates of the airmass vertical velocity [5, 6]. Here we describe methods for obtaining more precise estimates of the airmass vertical velocity that take into account energy transfer and sailplane acceleration. The methods are applied to flight data from a Perlan Project [7] flight in lee waves of the Sierra Nevada Mountains in California. The results are used to estimate the mountain wave structure relative to the upwind topography.

2 Theory

The airmass vertical velocity is estimated using post-flight logs of the recorded sailplane GPS-derived position and airspeed indicator-derived airspeed, together with the documented airspeed-sink rate characteristics of the sailplane. The airspeed data measured by the airspeed indicator, the indicated airspeed (IAS), deviates from the true airspeed (TAS) as a result of changes in air density at altitude. The indicated airspeed is converted to true airspeed using recorded temperature and/or pressure coupled with a model of the atmosphere as described in Ref. 5. The airmass vertical velocity is estimated as described in the next subsection. The horizontal

wind velocity is estimated as described in Ref. 5 and is briefly reviewed in the next subsection. Several methods for interpreting the airmass horizontal and vertical velocities in terms of the mountain wave structure are described in the final subsection.

2.1 Airmass Vertical Velocity Estimate

The airmass vertical velocity is estimated from the sailplane vertical velocity, and corrected for the static and dynamic forces acting. Given the sailplane vertical velocity v_v, sink rate s, and energy compensation e, the vertical velocity of the airmass v_{vw} is given by

$$v_{vw} = v_v + s - e. \tag{1}$$

Each of the three components are described below.

2.1.1 Vertical Velocity

The sailplane vertical velocity v_v is calculated from the GPS altitudes using second order central differences.

2.1.2 Sink Rate

The sink rate, s_0, of a sailplane at sea level (standard pressure and temperature) is given by the sailplane *flight polar* as a function of indicated airspeed and is provided in the sailplane flight manual. The flight polar applies to unbanked flight at a constant airspeed and wing loading. In banked or dolphin flight the wing load will increase or decrease and the flight polar is no longer meaningful.

For a particular IAS, v_a^{ind}, the sink rate depends on the altitude. However, the glide ratio $\operatorname{cosec}\gamma$, where γ is the angle between the airspeed vector and the horizontal, is independent of altitude. It is therefore convenient to work with the glide ratio versus IAS calculated from the flight polar as $\operatorname{cosec}\gamma = v_a^{ind}/s_0$. The sink rate s at altitude is then $s = v_a \sin\gamma = (v_a/v_a^{ind})s_0$, where v_a is the TAS (velocity relative to airmass at altitude) calculated as described in Ref. 5.

2.1.3 Energy Transfer

When the sailplane airspeed changes as a result of a change in elevator position, the sailplane climbs of descends. The change in vertical speed is a result of an exchange of potential and kinetic energy and not of vertical airmass motion. The change in sailplane vertical velocity that has occurred due to energy transfer should therefore be subtracted out. Equating the changes in kinetic and potential energy shows that the correction to be applied to the vertical speed is given by

$$e = -(v_a/g)(dv_a/dt), \tag{2}$$

where g is the acceleration due to gravity. The correction was calculated using finite differences with a time interval of 8 seconds.

2.1.4 Estimating G-forces

The flight polar applies only to unbanked flight at constant speed. Therefore, accurate estimates of the sailplane sink rate cannot be obtained directly when the aircraft is accelerating. Acceleration occurs either when the aircraft is turning (i.e. in banked flight) or in a pull-up or push-over manoeuver (sometimes called dolphin flight). Each of these produces a g-force different to 1.0. Although it may be possible to calculate sink rates under such circumstances, our current strategy is to estimate the g-force during the flight and exclude flight segments from the analysis for which it deviates from 1.0 by more than a given threshold.

During circling flight the sailplane is banked and the horizontal component of the lift force provides the centripetal force that depends on the speed and the radius of the turn. The turning radius is found by first determining the flight path relative to the airmass and fitting a circle using nonlinear least squares over 7 sequential positions. The flight path relative to the airmass is determined by adding $(\mathbf{v_g} - \mathbf{v_w})\Delta t$ to the previous position at each timestep, where $\mathbf{v_g}$ is the ground velocity from the GPS coordinates, $\mathbf{v_w}$ is the horizontal wind velocity determined as described in Section 2.2, and Δt is the time interval between GPS fixes. The centripetal force is then calculated from the glider mass, the turning radius and the airspeed.

For dolphin flight, a similar analysis is performed in the vertical, rather than the horizontal, plane. This gives a centripetal force in the vertical direction.

The circling and dolphin forces are orthogonal and the magnitude of the total force is calculated and denoted F_L. The g-force, denoted G, is then given by

$$G = F_L/mg. \tag{3}$$

If G deviates from unity by more than a threshold denoted δG then the polar is taken to be unreliable and the relevant point not used to estimate the airmass vertical velocity.

2.2 Horizontal Wind Estimate

The horizontal windspeed is not straightforwardly calculated without aircraft heading information, but a method that uses multiple GPS data and airspeed measurements is described in Ref. 5. Errors in the estimates are reduced by averaging over multiple data. Only certain data are suitable for estimating the horizontal windspeed and the flight path is divided into suitable regions, and the windspeed is estimated in each region [5].

2.3 Presentation of Results

The analysis described above produces estimates of the vertical and horizontal windspeeds at positions along the flight path. Since the flight path traverses a small region of the total volume of airspace in which the wave exists, the estimates obtained are a very sparse sampling of the wave structure. The problem addressed here is how to interpret this sparse dataset in terms of the atmospheric wave. The wave structure varies in the downwind direction relative to the mountain range and with altitude. We refer to the path of maximum altitude of the mountain range as the "ridge-line". Although the ridge-line is not precisely defined, an estimate of it is derived from digital topographical maps provided in the program See You [8].

The first method of displaying the results is suitable for flight segments that are primarily downwind of a particular point on the ridge-line. The airmass vertical velocity estimates are plotted versus distance downwind from the ridge-line, which shows the mountain wave relative to the surrounding topography. The streamlines of the mountain wave are expected to be approximately an exponentially damped sinusoid as a function of distance downwind. The airmass vertical velocity is the gradient of the streamlines which is also an exponentially damped sinusoid although phase-shifted relative to the streamlines. A damped sinusoid of the form

$$v_{vw}(x) = Be^{Cx}\cos(2\pi x/\lambda + D) + E, \qquad (4)$$

where x is the distance downwind from the ridge-line, λ is the wavelength, C is the damping coefficient, and D is the phase offset, is therefore fitted to the calculated airmass vertical velocity estimates.

The actual mountain wave streamlines are the integral of the vertical velocity and are represented and displayed as $w_{vw}(x)$ shifted by 90°. These plots show the wave relative to a cross section through the mountain range.

The second method of displaying the results is as a projection of the flight path and the ridge-line onto the horizontal plane with the flight path colour coded by the estimated airmass vertical velocity at each position on the flight path. This allows one to see the distribution of airmass vertical velocity relative to the topography. Interpretation is not particularly easy however, since the ridge-line is generally convoluted. A transformation is therefore made to a coordinate system (u, v) where u is the distance downwind from the ridge-line and v is the distance from a point on the ridge-line to the u-axis. Since the phase of the mountain wave is expected to be approximately fixed relative to the ridge-line, the display in the (u, v) coordinate system should show the wave structure more clearly.

The third method of displaying the results is used to show the wave structure with altitude. The flight path is colour coded with airmass vertical velocity and plotted in the (u, h) coordinate system where u is as defined above and h is altitude. This shows the position of the wave relative to the ridge-line as a function of altitude.

3 Results

Results are presented using data from Perlan Project [7] flight 039 flown in the lee waves of the Sierra Nevada Mountains in Southern California. The flight launched from California City (altitude 750m) at 2140Z on 24 April 2003 (1340 local time). Pilots were E. Enevoldson and S. Fossett. The flight lasted 5 hours and proceeded along the Owens Valley on the east of the Sierra Nevada Mountains to Big Pine and returned to California City.

There was extensive middle cloud upwind of the Sierra Nevadas and lenticular clouds were present in layers up to 14,000m. Large lee rotors were observed in the Owens Lake area. High altitude winds were moderate. Results are presented for the first 3.3 hours of the flight. The flight path is shown in figure 1.

The sailplane released from tow approximately 30 minutes after launch at an altitude of approximately 3,500m, and the air brakes were deployed at an altitude of approximately 7,000m approximately 30 minutes prior to landing. A maximum altitude of 13,044m was attained.

The sailplane was a production Glaser-dirks DG-505M specially equipped for high altitude flight and flown at an all up weight of 805kg (wing loading 44 kg/m^2). In addition to the usual instruments, the aircraft was fitted with a Volkslogger GPS positioning system and pressure transducer, a Borgelt B-50 airspeed indicator

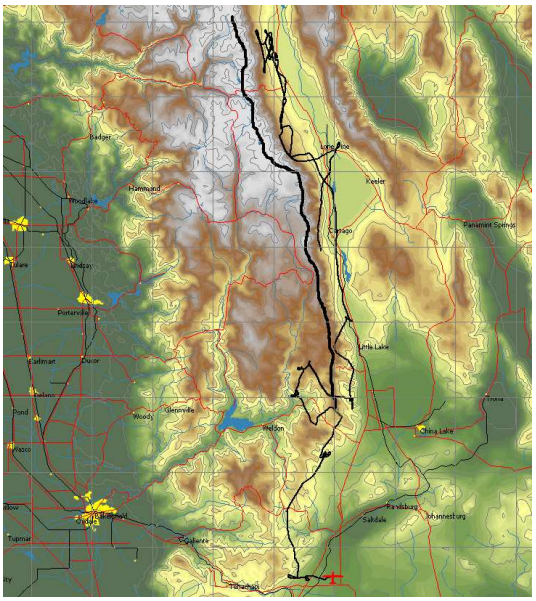

Figure 1: Flight path of 3.3 hours shown as the thin black line, and the ridge-line shown as the thick black line.

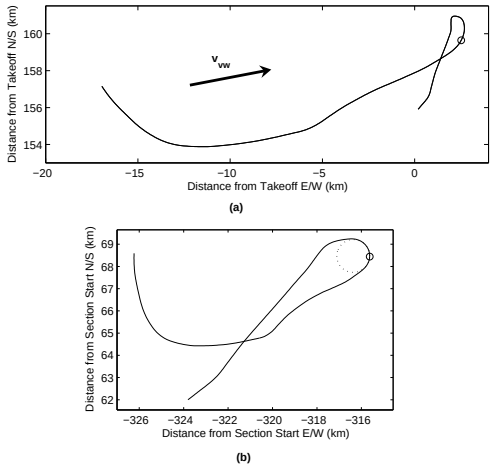

Figure 2: Flight segment $13150s < t < 13500s$, **(a)** flight path (relative to ground) with horizontal wind velocity vector $\mathbf{v_w}$, and **(b)** flight path (relative to the airmass) with a circle fitted to calculate the g-force.

and total energy compensated variometer, and a Platinum RTD (resistance temperature detector) outside air temperature probe. GPS fixes were obtained at 1 second intervals from the Volkslogger and pressure recordings made at 8 second intervals. Airspeed, variometer and temperature measurements were made at approximately 2.5 second intervals. All data were merged into a serial datastream and recorded on a custom datalogger. All data (except GPS fixes) were linearly interpolated onto the one-second GPS timestamps post flight. The sailplane glide ratio was measured as described in Ref. 5.

The GPS coordinates and airspeed were smoothed with a triangle window with a fwhm of 8 seconds. The airmass vertical velocity estimates were calculated as described in Section 2.1. The horizontal wind estimates were determined as in Ref. 5 and used to calculate the flight path relative to the airmass as described in Section 2.1. The flight path relative to the ground and to the airmass from a short flight segment are illustrated in figure 2. The circling radii and g-forces were calculated as described in Section 2.1 and samples for which $|G-1| > 0.07$ were not used to calculate the airmass vertical velocities. This corresponds to 5% of the flight.

The flight path traverses a long distance parallel to the mountain range in which the topography is highly complex with wide variations in altitude and width as shown in figure 1. The pilot intentionally flew in rising air when possible and traversed many different regions of the wave activity. This means the wave structure is not expected to be particularly evident for large sections of the flight. Therefore, small sections of the flight were interpreted using the methods described in Section 2.3, and then combined to give a profile of the wave.

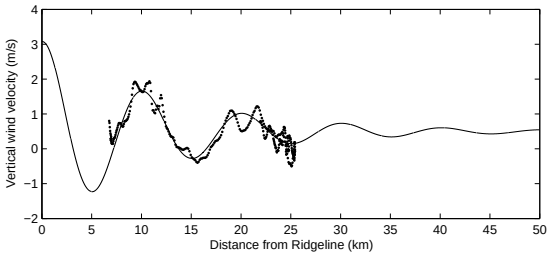

Figure 3: Airmass vertical velocity versus distance from the ridge-line for the flight segment $13150s < t < 13500s$ with the fitted sinusoid.

The only significant downwind segment of the flight ($13150s < t < 13500s$) is shown in figure 2a. The sailplane flew approximately 20km downwind of the same 6km section of ridge (south of Lone Pine). The average altitude of this section of flight is $13,000$m. Since the upwind section of the ridge is small, the effects of the varied topography are reduced in this flight segment. The estimates of the airmass vertical velocity are plotted versus distance downwind from the ridge-line in figure 3 and appear to display a wave structure. A least squares fit of Eq. 4 to the data is also shown in figure 3. The fit is quite good and gives a wavelength $\lambda = 10.5$ km.

The wave streamlines were calculated and are shown as curve **B**, together with a cross-section

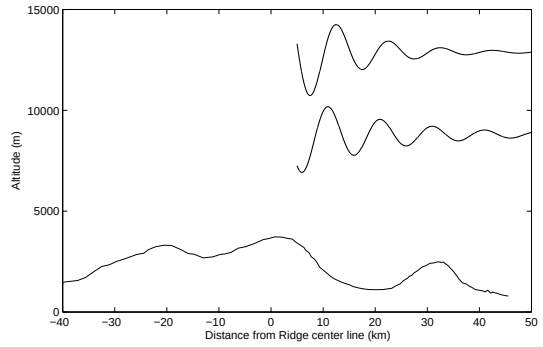

Figure 4: Topography cross section and interpreted wave streamlines **A** (8500s - 8800s) and **B** (13150s - 13500s).

through the topography, in figure 4. Another shorter flight segment (8500s - 8800s) is downwind of the same position on the ridge-line at an altitude of approximately $9,000$m and a similar analysis gave the streamlines shown as curve **A** in figure 4 with a wavelength of $\lambda = 10$ km.

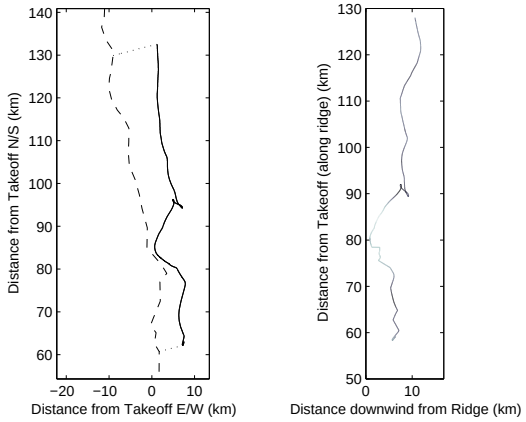

Figure 5: Flight section $6000s < t < 8000s$. **(a)** GPS flight path (solid line) and ridgeline (dashed line). **(b)** Airmass vertical velocity estimates (black indicates strong up and light grey indicates medium down) relative to the straightened ridge line.

A longer flight segment for $6000s < t < 8000s$ relative to the ridge-line is shown in figure 5a. The transformation to (u, v) coordinates was performed as described in Section 2.3 and the flight path is shown in figure 5b with the airmass vertical velocity estimates coded as black/grey as described in the caption. These results show the leading edge of the wave as the dark vertical segment between 5 and 10km from the ridge-line. They show that the short excursion of the flight upwind between 0 and 5km from the ridge took the sailplane out of the leading edge where the sailplane experienced much weaker airmass vertical velocities.

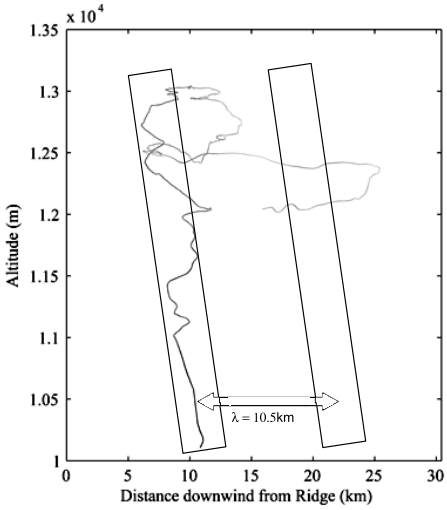

Figure 6: Airmass vertical velocities (coded black/grey as in figure 5) versus distance from the ridge-line and altitude for the flight segment $10000s < t < 13550s$.

A longer flight segment ($10000s < t < 13550s$) was investigated to see the wave structure as a function of altitude and relative to the ridge-line. Figure 6 shows the black/grey coded airmass vertical velocity in the (u, h) coordinate system. The regions of large vertical velocity are marked by the rectangles. This indicates that the leading edge of the wave is tilted upwind with increasing altitude. This is expected as a result of viscous drag [9]. The wave strength also decreases with altitude as is expected. A second, weaker wave crest is located approximately 10.5km downwind.

4 Discussion

The terrain has little influence on the wavelength, rather, it functions as an initial generator of the wave [4]. The induced oscillation has a natural frequency (the Brunt-Väisälä frequency) that depends on the temperature and temperature gradient [9]. The wavelength then depends on the natural frequency and the wind speed. Using the data for the flight, and the average ridge-line elevation of $3,200$m, the wavelength λ is calculated to be approximately 9km at the ridge height. This agrees reasonably well with the observed values of about 10km.

The atmospheric wave tends to be reinforced if the topography matches the wavelength, or if obstacles are present with spacings that are an integral number of wavelengths. It is interesting to note that two dominant ridges upwind are separated

by about 22km (approximately two wavelengths) and the first downwind ridge (the Inyo Mountain Range) is about 34km (approximately three wavelengths) downwind of the primary upwind ridge.

5 Conclusions

Methods have been developed for inverting basic sailplane flight data to obtain estimates of airmass vertical velocity along the flight path. Several methods have been developed to display and interpret the vertical and horizontal velocities in terms of mountain wave structure. Application of the method gives results that appear to be consistent with the calculated wavelength, and expected location of the wave relative to the topography.

The quality of the results obtained depends largely on the flight path taken by the sailplane pilot. More flight segments upwind or downwind would be more useful in this regard. This approach has potential for exploring mountain wave systems, particularly if flight paths are chosen with this objective in mind.

Acknowledgments

We are grateful to the Electrical and Computer Engineering Department at the UOC for a research grant, and NASA for support. Perlan Project flights are supported by the Steve Fossett Challenges.

References

[1] R. S. Scorer, *Dynamics of Meteorology and Climate*. New York: Wiley, 1997.

[2] G. A. Corby, "The airflow over mountains - a review of the state of current knowledge," *Quart. J. Roy. Meteor. Soc.*, vol. 80, pp. 491–521, 1954.

[3] T. P. Lane, M. J. Reeder, B. R. Morton, and T. L. Clark, "Observations and numerical modelling of mountain waves over the Southern Alps of New Zealand.," *Quart. J. Roy. Meteor. Soc.*, vol. 126, pp. 2765–2788, 2000.

[4] H. Reichmann, *Cross-Country Soaring*. Germany: Soaring Society of America Inc., 1993.

[5] R. P. Millane, R. G. Brown, E. Enevoldson, and J. E. Murray, "Estimating mountain wave windspeeds from sailplane flight data," in *Image Reconstruction from Incomplete Data III* (P. J. Bones, M. A. Fiddy, and R. P. Millane, eds.), vol. Proc. SPIE Vol. 5562, pp. 218–229, 2004.

[6] R. P. Millane, R. G. Brown, E. Enevoldson, and J. E. Murray, "Imaging mountain waves using sailplane flight data," in *Proceedings Image and Vision Computing New Zealand 2002*, pp. 285–290, 2004.

[7] E. J. Carter, E. H. Teets, and S. N. Goates, "The Perlan Project: New Zealand flights, meteorological support and modeling.," in *Proc. 19th Int. Cont. on IIPS, 83rd AMS Annual Meeting*, no. 1.2, 2003.

[8] See You: `http://www.SeeYou.ws`.

[9] R. B. Stull, *Meterology for Scientists and Engineers*. Pacific Grove: Brooks/Cole, 2 ed., 2000.